Dyes and Pigments 139 (2017) 403–411

Contents lists available at ScienceDirect

Dyes and Pigments

journal homepage: www.elsevier.com/locate/dyepig

# The effect of the length of alkyl side-chains on the molecular aggregation and photovoltaic performance of the isoindigo-based polymers

Xiai Sun [a], Zhiquan Zhang [a], Rongyan Hou [a], Meihua Huang [a, **], Bin Zhao [a, b, *], Songting Tan [b]

[a] College of Chemistry and Key Laboratory of Environmentally Friendly Chemistry and Applications of Ministry of Education, Xiangtan University, Xiangtan 411105, PR China
[b] Key Laboratory of Advanced Functional Polymeric Materials of College of Hunan Province, Xiangtan University, Xiangtan 411105, PR China

ARTICLE INFO

*Article history:*
Received 8 October 2016
Accepted 17 December 2016
Available online 19 December 2016

*Keywords:*
Polymer solar cells
Side-chain engineering
Isoindigo
Alkyl substituents
Structure-property relationship

ABSTRACT

To investigate the length of the alkyl side-chains on the photovoltaic performance, three isoindigo-based polymers with different-length side chains on the thiophene-benzene-thiophene (TBT) (electron-donating) moiety and isoindigo (electron-withdrawing) moiety have been designed and synthesized, in which the total carbon atom numbers of the side chains in a constitutional repeating unit are completely identical. The results indicate that the polymer with longer branched side chains on the TBT units and shorter linear side chains on the isoindigo units shows stronger interchain interaction and light-harvesting capacity in 1,2-dichlorobenzene solution and thin film, lower band gaps, stronger π−π stacking interaction, more appropriate microphase separation with $PC_{71}BM$, higher hole mobility and better photovoltaic performance. As a result, the bulk heterojunction (BHJ) device based on PTBTOD-IDB with 2-octyldodecyl on the TBT moiety and *n*-butyl on the isoindigo moiety exhibits a power conversion efficiency (PCE) of 5.29%, which is almost eight times as high as that of PTBTEH-IDHD with 2-ethylhexyl side chain on TBT moiety and 2-hexyldecyl side chain on isoindigo moiety.



## 1. Introduction

Polymer solar cells (PSCs) are a promising photovoltaic (PV) technology due to their potential application for low-cost flexible devices [1–4]. The power conversion efficiency (PCE), a key parameter to assess the performance of PSCs, has increased from 1% in the 1990s to over 11% just recently [5–10]. This impressive accomplishment is mainly achieved by the molecular engineering of the conjugated polymers [11–14], assisted by successes in interface modification and device optimization [15–18].

Recently, isoindigo (ID) has been considered as a remarkable electron-withdrawing moiety (A) because it is a symmetrical and perfect planar π-conjugated molecule, and its strong electron-deficient property leads to deep-lying energy levels of the lowest unoccupied molecular orbital (LUMO) and the highest occupied molecular orbital (HOMO) [19]. Several isoindigo-based co-polymers with different electron-donating moieties (D) have shown high photovoltaic performance [19–24]. Wang et al. developed an isoindigo-based polymer (P3TI), which gave a PCE of 6.3% [22]. We also reported a polymer with isoindigo moieties in the side chains (PBDT-TID) and achieved a PCE value of 6.51% [20]. Subsequently, Geng and his coworkers reported the polymer P(IID-DTC), combined with dithieno[3,2-*b*;6,7-*b*′]carbazole as D moieties and isoindigo as A moieties, and achieved a PCE value of 8.2% [25].

The role of the alkyl chains on a conjugated polymer are to confer solubility of the rigid-rod-like structure in common organic solvents, appropriate side chains not only improve solubility but also influence the intermolecular packing (aggregation), absorption spectra, blend film morphology, charge-carrier mobility, and energy levels of the conjugated polymers [21,26–30]. Therefore, more and more researchers focus on side-chain engineering to obtain high-performance photovoltaic materials [31–40]. On the one hand, the chemical structure of the side chains shows an impact on

* Corresponding author. College of Chemistry, Xiangtan University, Xiangtan 411105, PR China.
** Corresponding author. Tel./fax: +86 0731 58292251.
*E-mail addresses:* xtuhmh@163.com (M. Huang), xtuzb@163.com (B. Zhao).

http://dx.doi.org/10.1016/j.dyepig.2016.12.036
0143-7208/

energy levels which decides the open circuit voltage ($V_{oc}$) and PCE values [32,41]. Typically, after substituting alkoxy groups by alkyl groups, the polymer PBnDTDTBT achieved a deep-lying HOMO energy level of −5.40 eV [42]. When alkoxy groups were replaced by alkylthio side chains, the HOMO energy levels of the polymers were reduced, and the corresponding PSC device achieved an enhanced $V_{oc}$ [43–45]. On the other hand, the position of the alkyl side-chains and the position of alkyl chain branch position also play an important role in improving the photovoltaic performance of the polymers [27]. For examples, PDTSTTz-4 with a hexyl side chain on the 4-position of the thiophene units showed an order higher hole mobility ($7.8 \times 10^{-2}$ cm$^2$ V$^{-1}$ s$^{-1}$) [46] than PDTSTTz-3 with a hexyl side chain on the 3-position of thiophene units ($3.56 \times 10^{-3}$ cm$^2$ V$^{-1}$ s$^{-1}$) [47]. The McCulloch group reported that a longer distance between alkyl-chain branching position and the backbone led to stronger intermolecular π−π stacking, red-shifted absorption, improved hole mobility and better photovoltaic performance [31]. Recently the McGehee group gave an opinion that a more sterically accessible acceptor moiety and a more sterically hindered donor moiety would lead to a better photovoltaic performance [41]. Subsequently, So et al. reported that the polymer PBDT(EtHex)-TPD(Oct) with linear *n*-octyl side chain on TPD unit showed smaller π−π stacking distance, higher hole mobility and better photovoltaic performance than BDT(EtHex)-TPD(EtHex) with a bulkier ethylhexyl side chain [36]. Though a few references reported that a more sterically accessible acceptor moiety would lead to a higher photovoltaic performance, the length effect of the side chains on D moiety and A moiety was hardly discussed when the total carbon atoms number of the side chains in a constitutional repeating unit was fixed.

Herein, three isoindigo-based polymers, with different alkyl chain length on the thiophene-benzene-thiophene (**TBT**) (electron-donating) moiety and isoindigo (electron-withdrawing) moiety have been designed and synthesized. Firstly, the polymer **PTBTEH-IDHD** with 2-ethylhexyl side chain on **TBT** moiety and 2-hexyldecyl side chain on **ID** moiety was reported in our early work [48]. Then, the polymer **PTBTHD-IDEH** (Fig. 1) with 2-hexyldecyl side chain on **TBT** moiety and 2-ethylhexyl side chain on **ID** moiety was designed and synthesized, and the position effects of these two kinds of side chains on the photovoltaic performance was investigated. Finally, the side chain on **TBT** moiety was extended to 2-octyldodecyl and that on **ID** moiety was shortened to *n*-butyl to obtain the polymer **PTBTOD-IDB**. Among these polymers, the total carbon atom numbers of the side chains in a constitutional repeating unit remain unchanged in order to avoid the impact of the solubility difference derived from the length difference of side chains. The length and position effects of the alkyl side chain on light-harvesting capacity, band gaps, aggregation, the morphology and hole mobility of the blend film with $PC_{71}BM$, and photovoltaic performance of the PSC devices have been studied in detail.

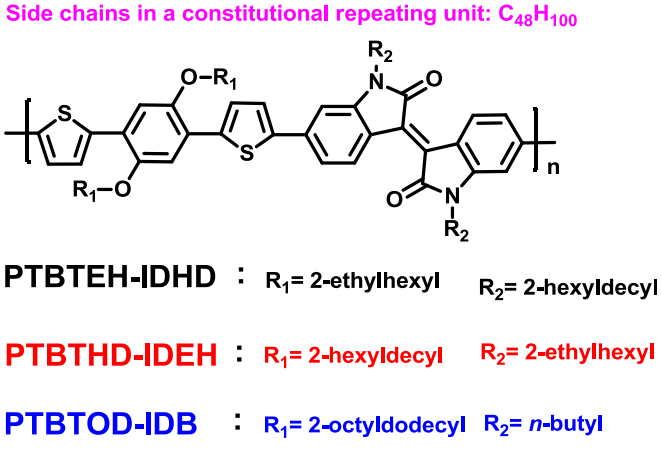


**Fig. 1.** The chemical structure of the polymers.

## 2. Experimental

### 2.1. Materials and chemicals

Tetrahydrofuran (THF) and toluene were refluxed over sodium and benzophenone, and distilled prior to use. DMF was dried and distilled under reduced pressure. All other materials, including the solvents and chemicals, were purchased from commercial suppliers (Aldrich, Energy Chemical, Alfa, *etc.*) and used without further purification unless stated otherwise.

### 2.2. Characterization

The NMR spectra were measured using Bruker AVANCE 400 MHz spectrometer. Mass spectra were measured using a Solarix FF-ICR-MS Analyzer in the MALDI mode. The elemental analysis result was characterized by Elementar VarioEL CHNS. Solution and thin film (on a quartz substrate) UV–vis absorption spectra were recorded using a Perkin-Elmer Lambda 25 spectrophotometer. Electrochemical measurements were carried out under nitrogen in a deoxygenated solution of tetra-*n*-butylammoniumhexafluorophosphate (0.1 M) in $CH_3CN$ using an electrochemical workstation with the polymer thin film on ITO (indium tin oxide) glass as the working electrode, Pt wire as the counter electrode, and $Ag/AgNO_3$ electrode as the reference electrode (100 mV s$^{-1}$). The potentials were referenced to ferrocene/ferrocenium couple by using ferrocene as an internal standard. Thermogravimetric analyses (TGA) were performed by using a Netzsch TG209 analyzer under nitrogen atmosphere at a heating rate of 20 °C min$^{-1}$. The average molecular weight and poly dispersity index (PDI) of the polymers were determined by Waters 1515 gel permeation chromatography (GPC) analysis with polystyrene as the standard. The nanoscale morphology of blended film was observed using a Digital Instruments Environ Scope atomic force microscope (AFM) in the tapping mode.

### 2.3. Fabrication and characterization of PSCs

The photovoltaic cells were constructed in a conventional sandwich structure of ITO/PEDOT:PSS(30 nm)/polymer: PCBM/LiF (0.4 nm)/Al (100 nm). The photosensitive blend layer of the polymers and PCBM was prepared by spin-coating the chlorobenzene solution (the polymer concentration is 15 mg mL$^{-1}$) onto the ITO/PEDOT:PSS (30 nm) electrode, and dried at room temperature for 30 min in a nitrogen-filled glove box. The cathode of the device, consisting of 0.4 nm of LiF and 100 nm of aluminum, was thermally deposited on the top of the blend film at $5 \times 10^{-4}$ Pa. The thickness of the active layer was measured by an Ambios Technology **XP-2** surface profilometer. Current density–voltage (*J*–*V*) characteristics were measured by a computer controlled Keithley 2600 source measurement under AM 1.5G illumination conditions, 100 mW cm$^{-2}$. The measurement of monochromatic incident photon-to-current conversion efficiency (IPCE) was performed by using a Zolix DCS300PA Data acquisition system. All these measurements were performed under ambient atmosphere at room temperature.

### 2.4. Synthetic processes

1,4-*Bis*(2-(5-trimethylstannyl)thienyl)-2,5-*bis*(2-ethylhexyloxy) benzene (**M1**), 1,4-*Bis*(2-(5-trimethylstannyl)thienyl)-2,5-*bis*(2-hexyldecyloxy)benzene (**M3**), 1,4-*Bis*(2-(5-trimethylstannyl) thienyl)-2,5-*bis*(2-octyldodecyloxy)benzene (**M5**) and **PTBTEH-IDHD** were synthesized according to the procedures reported by our group [48]. 6,6′-Dibromo-*N*,*N*′-(2- hexyldecyl)-isoindigo (**M2**), 6,6′-dibromo-*N*,*N*′-(2- ethylhexyl)-isoindigo (**M4**), 6,6′-dibromo-*N*,*N*′-(*n*-butyl)-isoindigo (**M6**) were synthesized by according to the literature procedures [22,49–52].

#### 2.4.1. 1,4-Bis(2-(5-trimethylstannyl)thienyl)-2,5-bis(2-hexyldecyloxy) benzene (*M3*)

To a solution of 1,4-dibromo-2,5-*bis*(2-hexyldecyloxy) benzene (1.50 g, 2.07 mmol) in dry tetrahydrofuran (THF, 30 mL), a solution of *n*-butyllithium in hexane (2.48 mL, 2.5 M) was added dropwise at −78 °C under argon atmosphere. The mixture was stirred for 30 min at −78 °C, then the resulting solution was warmed to room temperature and stirred for another 1 h. The mixture was cooled to −78 °C again, and trimethyltin chloride (6.21 mL, 6.21 mmol) in dry THF was added to the mixture. The mixture was stirred at −78 °C for 1 h and then stirred at room temperature overnight. The resulting mixture was poured into water (50 mL) and petroleum ether (100 mL). The organic layer was washed twice with water (50 mL) and dried over anhydrous $MgSO_4$. The organic layer was dried over vacuum to afford green solid. The solid was then purified by recrystallization from ethanol to give light green crystals (1.45 g, 66.7% yield). $^1$H NMR ($CDCl_3$, 400 MHz, $\delta$/ppm): 7.64 (d, $J$ = 3.1 Hz, 2H), 7.23 (s, 2H), 7.16 (d, $J$ = 3.2 Hz, 2H), 3.95 (d, $J$ = 5.1 Hz, 4H), 1.87 (m, 2H), 1.45–1.26 (m, 48), 0.88 (t, $J1$ = 6.1 Hz, $J2$ = 6.7 Hz, 12H), 0.36 (t, $J1$ = 28.1 Hz, $J2$ = 28.2 Hz, 18H). $^{13}$C NMR ($CDCl_3$, 100 MHz, $\delta$/ppm):149.31, 145.43, 137.51, 134.99, 126.62, 122.91, 112.80, 72.26, 38.32, 31.97, 31.93, 31.58, 30.14, 29.79, 29.68, 29.41, 27.04, 26.99, 22.74, 14.17, −8.25. FT-ICR MS ($C_{52}H_{90}O_2S_2Sn_2$) $[M]^+$ $m/z$: calcd for 1048.4431; found 1048.4430. Elemental anal. calcd. for ($C_{52}H_{90}O_2S_2Sn_2$): C, 59.55; H, 8.65; S, 6.11. Found: C, 59.30; H, 8.77; S, 6.30.

#### 2.4.2. 6,6′-Dibromo-N,N′-(2-ethylhexyl)-isoindigo (*M4*)

To a solution of 6,6′-dibromo-isoindigo (2.0 g, 4.76 mmol) in *N*,*N*-dimethyl formamide (DMF, 100 mL), tetrabutylammonium bromide (0.1 g) and $K_2CO_3$ (3.95 g, 28.56 mmol) were added quickly under argon atmosphere. The mixture was stirred at 80 °C for 30 min, then the solution of 1-bromo-2-ethylhexane (2.30 g, 11.90 mmol) in DMF (30 mL) was added. The mixture was stirred overnight. After cooling to room temperature, it was filtered, and the filtrate was extracted by $CH_2Cl_2$ and washed with brine. The organic layer was dried over anhydrous magnesium sulfate, and then filtered. After removed the solvent by a rotary evaporator, the crude product was obtained, and it was further purified by column chromatography using petroleum ether/$CH_2Cl_2$ (3:1, v:v) as the eluent to yield a dark red solid (1.68 g, 54.5%). $^1$H NMR (400 MHz, $CDCl_3$, $\delta$/ppm):9.04 (d, $J$ = 8.5 Hz, 2H), 7.16 (dd, $J1$ = 1.4 Hz, $J2$ = 8.5 Hz, 2H), 6.90 (d, $J$ = 1.4 Hz, 2H), 3.63 (m, 4H), 1.84–1.81 (m, 2H), 1.43–1.26 (m, 16H), 0.95–0.91 (m, 12H). $^{13}$C NMR (100 MHz, $CDCl_3$, $\delta$/ppm): 168.07, 146.15, 132.55, 131.01, 126.69, 125.12, 120.36, 111.54, 44.37, 37.43, 30.58, 28.58, 23.99, 23.08, 14.09, 10.66. FT-ICR MS ($C_{32}H_{40}Br_2N_2O_2$) $[M]^+$ $m/z$:calcd for 643.1529; found 643.1530. Elemental anal. calcd. for ($C_{32}H_{40}Br_2N_2O_2$): C, 59.64; H, 6.26; N, 4.35. Found: C, 59.48; H, 6.34; N, 4.38.

#### 2.4.3. 1,4-Bis(2-(5-trimethylstannyl)thienyl)-2,5-bis(2-octyldodecyloxy) benzene (*M5*)

To a solution of 1,4-dibromo-2,5-*bis*(2-octyldodecyloxy) benzene (3.05 g, 3.65 mmol) in dry THF (30 mL), a solution of *n*-butyllithium in hexane (4.38 mL, 2.5 M) was added dropwise at −78 °C under argon atmosphere. The mixture was stirred for 30 min at −78 °C, then the resulting solution was warmed to room temperature and stirred for another 1 h. The mixture was cooled to −78 °C again, and trimethyltin chloride (10.95 mL, 10.95 mmol) in dry THF was added to the mixture. The mixture was stirred at −78 °C for 1 h and then stirred at room temperature overnight. The resulting mixture was poured into water (50 mL) and petroleum ether (100 mL). The organic layer was washed twice with water (50 mL) and dried over anhydrous $MgSO_4$. The organic layer was dried over vacuum to afford green solid. The solid was then purified by recrystallization from ethanol to give light green crystals (1.89 g, 44.7% yield). $^1$H NMR (400 MHz, $CDCl_3$, $\delta$/ppm): 7.64 (d, $J$ = 3.3 Hz, 2H), 7.23 (s, 2H), 7.18 (d, $J$ = 3.4 Hz, 2H), 3.96 (d, $J$ = 5.3 Hz, 4H), 1.89 (m, 2H), 1.45–1.25 (m, 64H), 0.89–0.86 (t, $J1$ = 6.2 Hz, $J2$ = 6.9 Hz, 12H), 0.46–0.32 (t, $J1$ = 28.4 Hz, $J2$ = 28.5 Hz, 18H). $^{13}$C NMR (100 MHz, $CDCl_3$, $\delta$/ppm): 149.28, 145.41, 137.79, 134.98, 126.60, 122.86, 112.72, 72.23, 38.30, 31.98, 31.56, 30.14, 29.76, 29.72, 29.69, 29.42, 27.04, 22.74, 14.18, −8.24. FT-ICR MS ($C_{60}H_{106}O_2S_2Sn_2$) $[M]^+$ $m/z$: calcd for 1160.5686; found 1160.5690. Elemental anal. calcd. for ($C_{60}H_{106}O_2S_2Sn_2$): C, 62.07; H, 9.20; S, 5.52. Found: C, 61.87; H, 9.28; S, 5.45.

### 2.5. 6,6′-Dibromo-N,N′-(n-butyl)-isoindigo *M6*

To a solution of 6,6′-dibromo-isoindigo (2.0 g, 4.76 mmol) in DMF (100 mL), tetrabutylammonium bromide (0.1 g) and $K_2CO_3$ (3.95 g, 28.56 mmol) were added quickly. The mixture was stirred at 80 °C for 30 min, then the solution of 1-bromo-2-butane (1.63 g, 11.90 mmol) in DMF (30 mL) was added under argon atmosphere. The mixture was stirred overnight. After cooling to room temperature, it was filtered, and the filtrate was extracted by $CH_2Cl_2$ and washed with brine. The organic layer was dried over anhydrous magnesium sulfate, and then filtered. After removed the solvent by a rotary evaporator, the crude product was obtained, and it was further purified by column chromatography using petroleum ether/$CH_2Cl_2$ (2:1, v:v) as the eluent to yield a dark red solid (1.19 g, 47.1%). $^1$H NMR (400 MHz, $CDCl_3$, $\delta$/ppm):9.07 (d, $J$ = 8.6 Hz, 2H), 7.16 (dd, $J1$ = 1.4 Hz, $J2$ = 8.5 Hz, 2H), 6.93 (d, $J$ = 1.1 Hz, 2H), 3.73 (t, $J1$ = 7.3 Hz, $J2$ = 7.3 Hz, 4H), 1.46–1.37 (m, 8H), 0.99–0.96(t, J1 = 7.3 Hz, J2 = 7.3 Hz, 6H) $^{13}$C NMR (100 MHz, $CDCl_3$, $\delta$/ppm): 167.74, 145.77, 132.66, 131.20, 126.75, 125.15, 120.40, 111.33, 40.03, 29.46, 20.28, 13.79. FT-ICR MS ($C_{24}H_{24}Br_2N_2O_2$) $[M]^+$ $m/z$:calcd for 531.0277; found 531.0279. Elemental anal. calcd. for ($C_{24}H_{24}Br_2N_2O_2$): C,54.16; H, 4.54; N, 5.26. Found: C, 54.03; H, 4.63; N, 5.34.

### 2.6. Polymerization of *PTBTOD-IDB*

**M5** (184.8 mg, 0.16 mmol) **M6** (84.72 mg, 0.16 mmol) were dissolved into toluene (8 mL) in a 25 mL flask under argon protection. The solution was flushed with argon for 10 min, and then 5.52 mg of $Pd(PPh_3)_4$ was added into the flask. The solution was flushed with argon for 10 min again, then it was stirred at 100 °C for 48 h under argon atmosphere. After cooled to room temperature, the mixture was poured into methanol (200 mL). The precipitated solid was collected and purifled by Soxhlet extraction with methanol, acetone, petroleum ether and chloroform in sequence. The title polymer was obtained as a dark green solid (110 mg, yield 57.38%). $^1$H NMR (400 MHz, $CDCl_3$, $\delta$/ppm): 9.25–9.15 (br), 7.71–7.00 (br), 4.14–3.83 (br), 2.03–1.92(br), 1.70–0.80 (br). $\overline{M_n}$ (Number-average molecular weight) = 19 kDa, PDI = 2.00.

### 2.7. Polymerization of *PTBTHD-IDEH*

**PTBTHD-IDEH** was prepared using the similar procedure as **PTBTOD-IDB** with the monomers **M3** and **M4** as a dark green solid (165 mg, yield 70.16%).$^1$H NMR (400 MHz, $CDCl_3$, $\delta$/ppm): 9.24–8.91 (br, 2H), 7.71–6.95 (br, 10H), 4.30–4.28 (br, 4H), 4.09–4.04 (br, 4H), 2.05–1.87 (br, 4H), 1.71–0.80 (br, 88H). $\overline{M_n}$ = 16 kDa, PDI = 1.71.

## 3. Results and discussion

### 3.1. Synthesis and chemical characterization

The synthetic routes for the polymers are shown in Scheme 1. The structures of the monomers **M3-M6** were confirmed by $^1$H NMR, $^{13}$C NMR, elemental analysis, FT-ICR MS. The polymers were prepared through Stille coupling reaction between the electron-donating monomer and the electron-withdrawing monomer as shown in Scheme 1. The polymerization results of the polymers are summarized in Table 1. As shown in Table 1, the $\overline{M_n}$ s and the polydispersity indexes (PDI), determined by gel permeation chromatography (GPC) using chloroform as the eluent, are 16 kDa and 1.57 for **PTBTEH-IDHD**, 16 kDa and 1.71 for **PTBHD–IDEH**, 19 kDa and 2.00 for **PTBTOD–IDB**, respectively. Usually, the molecular weight has a strong impact on the solubility of the polymer in organic solvents. Therefore, **PTBTEH-IDHD** and **PTBTHD-IDEH** show good solubility in THF, chloroform, chlorobenzene and 1,2-dichlorobenzene (*o*-DCB) because of their low molecular weight. However, **PTBTOD-IDB** exhibits a poor solubility in THF for its high molecular weight, but it shows good solubility in chloroform, chlorobenzene and *o*-DCB.

### 3.2. Thermal properties

The thermal properties of the polymers were investigated by TGA. As shown in Fig. S1 and Table 1, the TGA curves reveal that the onset temperatures with 5% weight loss ($T_d$) of **PTBTEH-IDHD**, **PTBTHD-IDEH**, and **PTBTOD-IDB**, are 401 °C, 387 °C, 378 °C, respectively. Obviously, the thermal stability of these polymers is sufficient for the applications in optoelectronic devices.

### 3.3. Optical properties

The optical properties of the polymers were investigated by UV–Vis absorption spectroscopy. Fig. 2 shows the absorption spectra of **PTBTEH-IDHD**, **PTBTHD-IDED**, and **PTBTOD-IDB** in diluted *o*-DCB solution (Fig. 2a) and thin film on a quartz substrate (Fig. 2b), and the corresponding data are summarized in Table 2. As shown in Fig. 2a, all the polymers exhibit two distinct absorption bands. The first absorption band in shorter wavelengths region

**Table 1**
Molecular weights and thermal properties of the polymers.

| Polymers | Yield (%) | $\overline{M_n}$(kDa)[a] | PDI | $T_d$ (°C)[b] |
|---|---|---|---|---|
| **PTBTEH-IDHD** | 62 | 16 | 1.57 | 401 |
| **PTBTHD-IDEH** | 70 | 16 | 1.71 | 387 |
| **PTBTOD-IDB** | 57 | 19 | 2.00 | 378 |

[a] Determined by GPC with chloroform as the eluent.
[b] Decomposition temperature, determined by TGA in nitrogen with 5% weight loss.

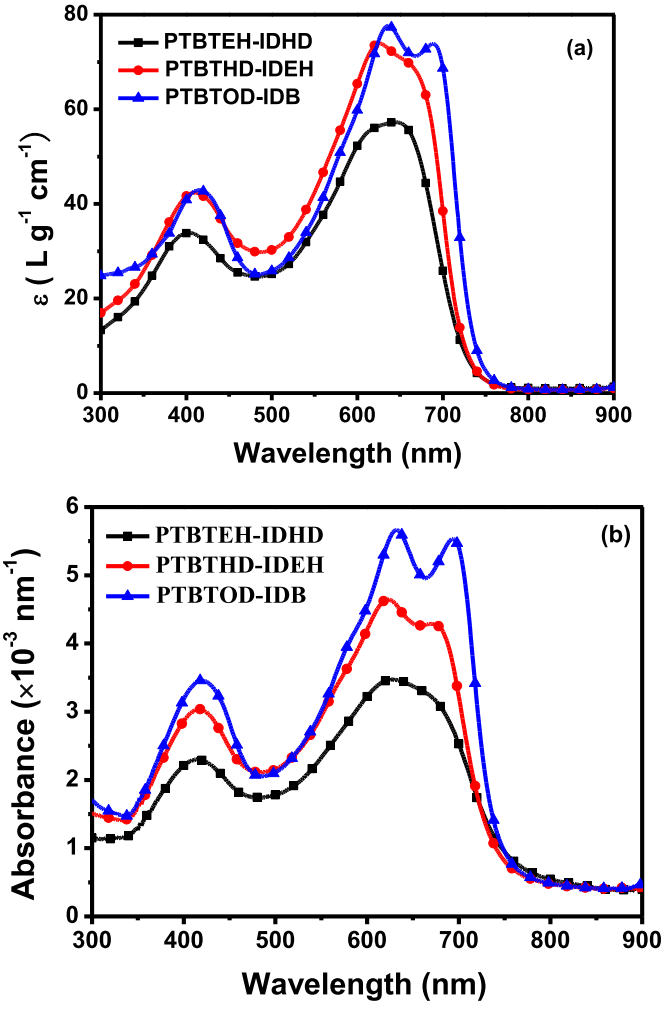


**Fig. 2.** UV–Vis absorption of the polymers in the *o*-DCB solution (a) and thin films (b).

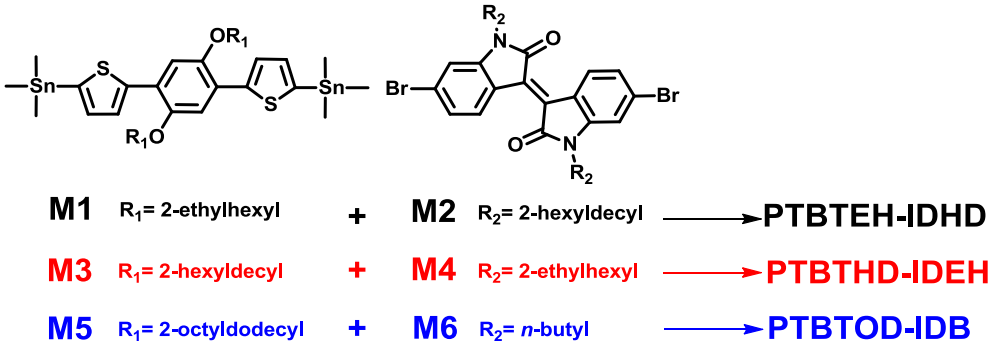


**Scheme 1.** Synthesis of the polymers.

**Table 2**
Optical and electrochemical properties of the polymers.

| Polymers | Solution $\lambda_{s,\ max}$ (nm) [a] | Film $\lambda_{f,\ max}$ (nm) | Film $\lambda_{edge}$ (nm) | $E_g^{opt}$ (eV)[b] | HOMO (eV) | LUMO (eV) | $E_g^{ec}$ (eV) |
|---|---|---|---|---|---|---|---|
| **PTBTEH-IDHD** | 646 | 628 | 753 | 1.65 | −5.47 | −3.48 | 1.99 |
| **PTBTHD-IDEH** | 626 | 624 | 734 | 1.69 | −5.47 | −3.60 | 1.87 |
| **PTBTOD-IDB** | 636 | 632 | 739 | 1.68 | −5.21 | −3.61 | 1.60 |

[a] Dilute *o*-DCB solution.
[b] Band gap estimated from the optical absorption band edge of the films.

(350–500 nm) with the absorption peak wavelength at 403 nm for **PTBTEH-IDHD**, 410 nm for **PTBTHD-IDED**, 416 nm for **PTBTOD-IDB**, which is attributed to the localized π–π* transition. The other absorption band in longer wavelengths (500–900 nm), is attributed to the intramolecular charge transfer (ICT) between the electron-donating and electron-withdrawing units [53] and the interchain interaction [54]. It is noted that **PTBTEH-IDHD** and **PTBTHD-IDEH** only show the shoulder peaks between 650 and 680 nm, but **PTBTOD-IDB** exhibits an obvious peak at 689 nm. This result implies **PTBTOD-IDB** should possess the strongest molecular aggregation in the solution.

To better understand the effects of the side chains on the interchain interaction in diluted *o*-DCB solution, the temperature-dependent UV–Vis absorption spectra was characterized and shown in Fig. S2. As shown in Fig. S2, the absorption spectra of **PTBTEH-IDHD**, **PTBTHD-IDEH**, and **PTBTOD-IDB** exhibit a gradually increased red-shift when their *o*-DCB solution is lowered from 95 °C to 25 °C. These results indicate that the polymers possess stronger molecular aggregation in *o*-DCB solution with the increase of side chain length on the electron-donating unit and decrease of side chain length on electron-withdrawing unit. According to Fig. 2a, the maximum absorption coefficients are 57, 74, and 78 L $g^{-1}$ $cm^{-1}$ for **PTBTEH-IDHD**, **PTBTHD-IDEH**, and **PTBTOD-IDB**, respectively. Compared with the former two polymers, **PTBTOD-IDB** shows larger absorption coefficient, which indicates it possesses the strongest light harvesting capacity than the other polymers under the same applied conditions. Compared with the absorption spectra in solution, the maximum absorption peaks ($\lambda_{f,\ max}$) are blue–shifted to 628, 624, 632 nm for **PTBTEH-IDHD**, **PTBTHD-IDEH**, and **PTBTOD-IDB**, respectively, and a shoulder peak between 660 nm and 700 nm becomes increasingly clear which is a π–π interaction. It is noticed that the absorbance (absorption intensity per unit thickness) of the maximum absorption peak increases in accordance with the order of **PTBTEH-IDHD**, **PTBTHD-IDEH**, and **PTBTOD-IDB**, which indicates that the light harvesting capacity of the polymer increases with increase of side chain length on the electron-donating unit and decrease of side chain length on electron-withdrawing unit. Simultaneously, the absorbance of the shoulder peak between 660 nm and 700 nm conforms to the same regularity. In other words, with the increase of side chain length on the electron-donating unit and decrease of side chain length on electron-withdrawing unit, the polymer shows more and more ordered aggregation and stronger π–π stacking interaction. Usually, the enhanced π–π stacking is beneficial to inter-chain charge transport, so the **PTBTOD-IDB** film should possess a higher hole mobility than **PTBTEH-IDHD** and **PTBTHD-IDEH** film, which leads to better photovoltaic performance in polymer solar cells. According to the absorption spectra of the films (Fig. 2b), the optical band gaps of the polymers, calculated from the onset of optical absorption $\lambda_{edge}$(nm), are 1.65 eV for **PTBTEH-IDHD**, 1.69 eV for **PTBTHD-IDEH** and 1.68 eV for **PTBTOD-IDB**, respectively (Table 2).

Fig. 3 presents the photoluminescence (PL) spectra of the pristine polymer films and the blend films with $PC_{71}BM$ (100 nm). As shown in Fig. 3, there is an obvious fluorescence quenching in every blend film, which indicates there is an effective electron transport from every polymer to $PC_{71}BM$. It is noticed that the **PTBTEH-IDHD**, **PTBTHD-IDEH** and **PTBTOD-IDB** blend films retains 12.8%, 5.9% and 2.8% fluorescence intensity compared with the corresponding pristine film, respectively. That is to say, **PTBTOD-IDB** can achieve the most effective electron transport to $PC_{71}BM$, but **PTBTEH-IDHD** only possesses the most inferior electron transport ability to $PC_{71}BM$ in three polymers. The result implies that the **PTBTOD-IDB**-based PSC device would possess the highest short-circuit current density ($J_{sc}$) value.

### 3.4. Electrochemical properties

The HOMO and LUMO energy levels can be estimated from the onset oxidation potential ($E_{ox}$) and the onset reduction potential ($E_{red}$) according to cyclic voltammetry (CV) measurements, respectively [55]. The cyclic voltammetry were recorded using ITO glass as the working electrode, $Ag/AgNO_3$ electrode as the reference and Pt wire as the counter electrode. Fig. 4 shows the CV curves of ferrocene and the polymers. It can be seen that the redox potential of the ferrocene/ferrocenium couple is 0.14 V vs. $Ag/Ag^+$, corresponding to the absolute energy level under vacuum (−4.80 eV). Thus, the HOMO and LUMO energy levels as well as the

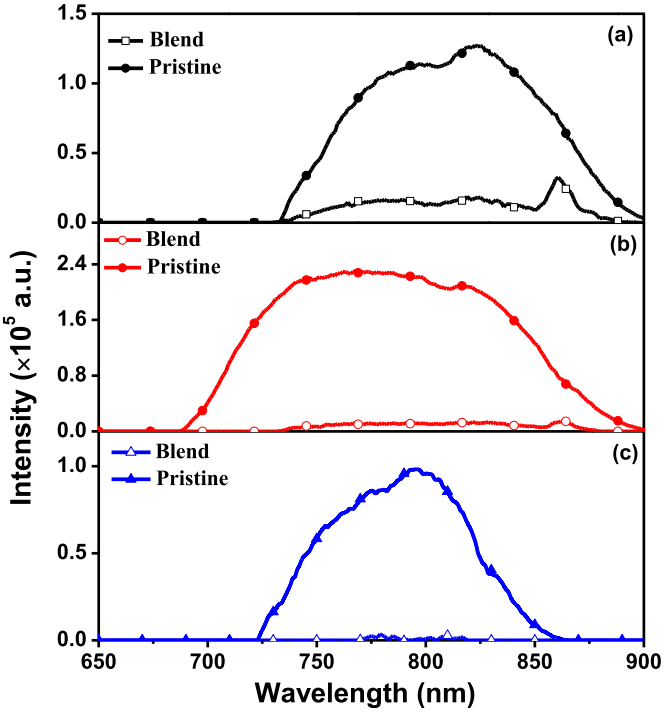


**Fig. 3.** Photoluminescence spectra of the polymers (a) **PTBTEH-IDHD**, (b) **PTBTHD-IDEH**, (c) **PTBTOD-IDB** and the corresponding blend films with $PC_{71}BM$.

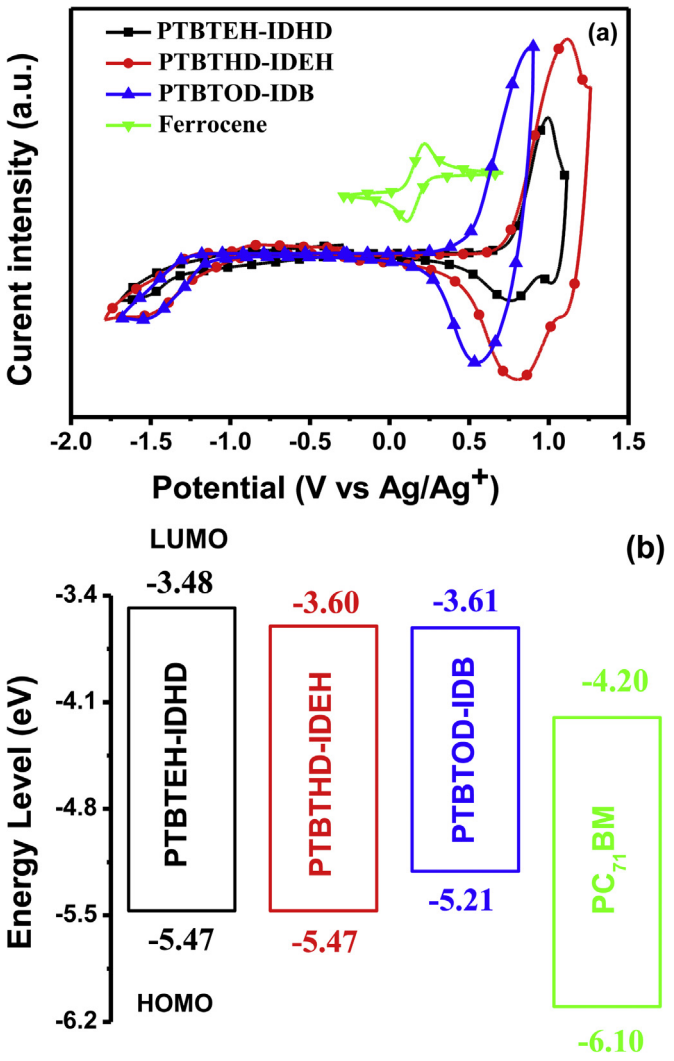


**Fig. 4.** (a) Cyclic voltammograms of ferrocene and the polymer films with a scan rate of 100 mV $s^{-1}$ and (b) energy diagrams of **PTBTEH-IDHD**, **PTBTHD-IDEH**, **PTBTOD-IDB** and $PC_{71}BM$.

electrochemical energy gaps ($E_g^{ec}$) of the polymers were calculated according to the following equations:

$$\text{HOMO} = -\text{e}\,(E_{ox} + 4.66)\ (\text{eV}) \quad (1)$$

$$\text{LUMO} = -\text{e}\,(E_{red} + 4.66)\ (\text{eV}) \quad (2)$$

$$Eec\ g = \text{e}\,(E_{ox} - E_{red})\ (\text{eV}) \quad (3)$$

The onset potentials for oxidation ($E_{ox}$) were observed to be 0.81, 0.81, and 0.55 V for **PTBTEH-IDHD**, **PTBTHD-IDEH**, and **PTBTOD-IDB**, respectively. Accordingly, the HOMO energy levels are −5.47 eV for **PTBTEH-IDHD**, −5.47 eV for **PTBTHD-IDEH** and −5.21 eV for **PTBTOD-IDB**. Usually, a deep HOMO energy level leads to good air stability and a high $V_{oc}$ for the PSCs [56]. In addition, the onset potentials for reduction ($E_{red}$) of them were found to be −1.18, −1.06 and −1.05 V, respectively. Clearly, all the LUMO energy levels are −3.48 eV for **PTBTEH-IDHD**, −3.60 eV for **PTBTHD-IDEH** and −3.61 eV for **PTBTOD-IDB**. Obviously, all the LUMO levels of the polymers are much higher than the LUMO level of the $PC_{71}BM$ acceptor (−4.2 eV), which ensures energetically favorable electron transfer.

According to the HOMO levels and the LUMO levels, the electrochemical band gaps of the polymers are calculated to be 1.99 eV for **PTBTEH-IDHD**, 1.87 eV for **PTBTHD-IDEH**, 1.60 eV for **PTBTOD-IDB**. As shown in Table 2, the discrepancy between the optical and electrochemical band gaps might be induced by the presence of an energy barrier at the interface between the polymer film and the electrode surface [57].

### 3.5. X-ray diffraction

To investigate the effect of the side chains on the molecular aggregation of the polymers, wide angle X-ray diffraction (WAXRD) of the polymer films was performed with Cu-Kα radiation (Fig. 5). As shown in Fig. 5, every polymer exhibits a distinct diffraction peak in the small angle region of 4–6° and another broad one in the large angle range between 15 and 28°. The WAXRD clearly shows 100 diffraction peaks at 4.79° for **PTBTEH-IDHD**, 4.39° for **PTBTHD-IDEH**, and 4.24° for **PTBTOD-IDB**, corresponding to the lamellar distance of 18.43 Å, 20.10 Å, and 20.82 Å, respectively, which indicates that the polymer possesses larger lamellar distances with the extension of side chains on TBT moieties. Synchronously, the 010 diffraction peaks are observed at 21.94° for **PTBTEH-IDHD**, 22.22° (19.67°) for **PTBTHD-IDEH**, and 22.25° (20.41°) for **PTBTOD-IDB**, indicating the π−π stacking distances of 4.05 Å, 4.00 (4.51) Å, and 3.99 (4.35) Å, respectively. Compared with the **PTBTEH-IDHD**, the **PTBTHD-IDEH** and **PTBTOD-IDB** films show obviously larger diffraction peaks and extra 200 diffraction peak as well as 300 diffraction peaks, which indicates that **PTBTHD-IDEH** and **PTBTOD-IDB** possess more orderly molecular aggregation and better crystallization ability than **PTBTEH-IDHD** [58]. Simultaneously, the **PTBTHD-IDEH** and **PTBTOD-IDB** films exhibits two 010 diffraction peaks, which indicates there are two kinds of π−π stacking patterns in the two polymer films. Besides, the **PTBTOD-IDB** film shows higher 010 diffraction peaks than the **PTBTHD-IDEH** film, indicating the stronger π−π stacking interaction of **PTBTOD-IDB**. Obviously, the polymer exhibits higher crystallization ability and stronger π−π stacking interaction with increasing the length of the branched side chains on the D moieties and shortening the length of the side chains on the A moieties at the same time. All of these results imply that **PTBTOD-IDB** and **PTBTHD-IDEH** would possess higher hole mobility than **PTBTEH-IDHD**, which is beneficial to improving the $J_{sc}$ and PCEs values in PSCs.

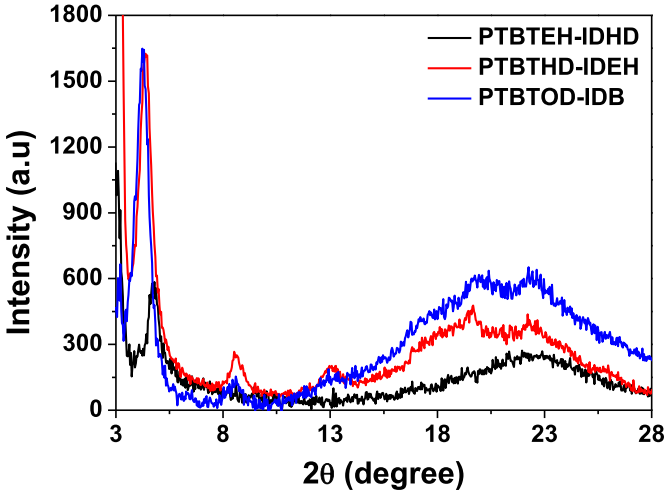


**Fig. 5.** WAXRD analysis of the polymer films.

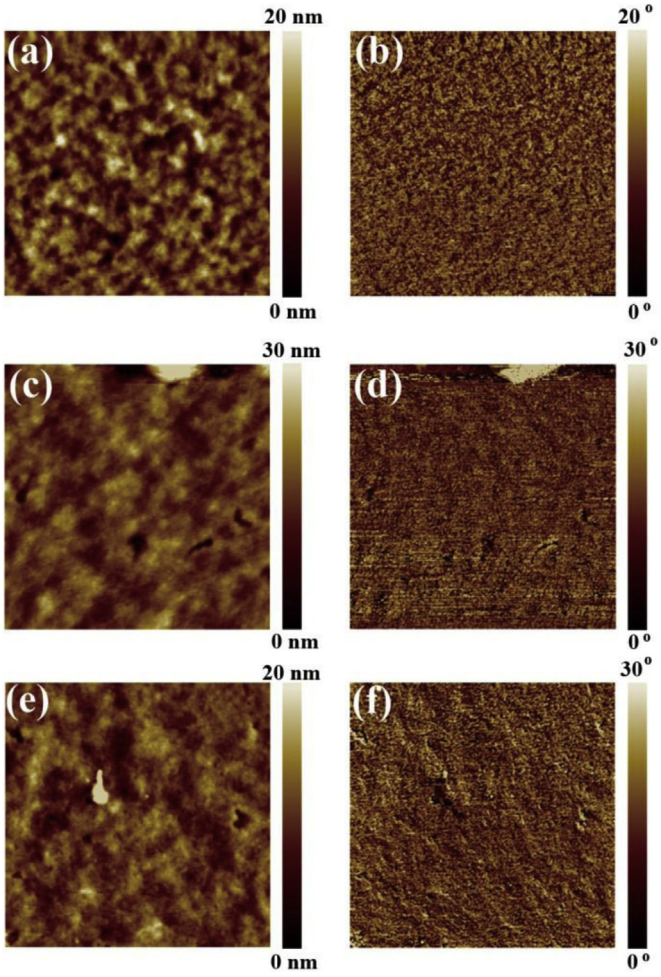


**Fig. 6.** AFM height and phase images (tapping-mode, 3 × 3 μm) for the polymers: $PC_{71}BM$ blend films (w/w 1:1.5). (a) and (b): **PTBTEH-IDHD**, (c) and (d): **PTBTHD-IDEH**, (e) and (f): **PTBTOD-IDB**.

### 3.6. Morphology

The morphology of the blend film is a critical factor for determining the photovoltaic property of a PSC device, so the morphology of the blend films (polymer: $PC_{71}BM$; 1:1.5) was investigated by atomic force microscopy (AFM) and shown in Fig. 6. As shown in Fig. 6, the **PTBTEH-IDHD** blend film shows obvious phase separation, and the domain size is obviously larger than those of the other blend films. However, the **PTBTOD-IDB** blend film shows the smoothest surface and the most appropriate microphase separation, and the domain size is smaller than that of the **PTBTEH-IDHD** and **PTBTHD-IDEH** blend films. Besides, the **PTBTOD-IDB** blend film presents a nanoscale fibril conformation. These results evidence that the polymer with longer branched alkyl side chains on the D moieties and shorter linear alkyl side chains on the A moieties (**PTBTOD-IDB**) possesses better miscibility with **PCBM**, and the corresponding blend film is easy to form a smaller domain size and better bicontinuous microphase separation. The blend films exhibit the RMS (surface root mean square roughness) values of 3.88 nm for **PTBTEH-IDHD**, 2.86 nm for **PTBTHD-IDEH** and 2.85 nm for **PTBTOD-IDB**. A smaller domain size and better bicontinuous microphase separation would be beneficial to more effective charge separation, higher charge mobility, larger $J_{sc}$ as well as PCE values [59].

### 3.7. Hole mobility

The hole mobilities of the polymer/$PC_{71}BM$ blend films were measured by using the space charge limit current (SCLC) method with the configuration of ITO/PEDOT: PSS (30 nm)/polymer: $PC_{71}BM$/$MoO_3$ (10 nm)/Al (100 nm) and summarized in Table 3. As discussed before, **PTBTOD-IDB** possesses the strongest π−π stacking interaction, and its blend film possesses the most appropriate bicontinuous microphase separation. Therefore, the **PTBTOD-IDB** blend film shows the highest hole mobility of $2.5 \times 10^{-4}$ $cm^2$ $V^{-1}$ $s^{-1}$, which is seven times higher than that of the **PTBTHD-IDEH** blend film ($3.4 \times 10^{-5}$ $cm^2$ $V^{-1}$ $s^{-1}$) and almost three orders of magnitude higher than that of the **PTBTEH-IDHD** blend film ($4.2 \times 10^{-7}$ $cm^2$ $V^{-1}$ $s^{-1}$).

### 3.8. Photovoltaic properties

The bulk heterojunction PSCs were fabricated with a conventional sandwich structure of ITO/PEDOT:PSS (30 nm)/polymer: PCBM/LiF (0.4 nm)/Al (100 nm). In the first place, the PSCs devices based on the polymers and $PC_{61}BM$ were fabricated, and the current density−voltage (*J-V*) curves are shown in Fig. S3 and the corresponding photovoltaic parameters are listed in Table S1. The preliminary optimized weight ratio of the blend film was obtained as polymer: PCBM = 1:1.5. Subsequently, the current *J-V* curves of the PSC devices with $PC_{71}BM$ were characterized and shown in Fig. 7, and the corresponding photovoltaic parameters are listed in Table 3. As shown in Fig. 7, the **PTBTHD-IDEH** device shows the largest $V_{oc}$ value (0.87 V), which is higher than that of the **PTBTOD-IDB** device (0.81 V). It is reasonable that **PTBTHD-IDEH** possesses a slightly lower-lying HOMO energy level (−5.47 eV) than that of **PTBTOD-IDB** (−5.21 eV). It is noticed that the **PTBTOD-IDB** device exhibits a lower photon energy loss of 0.79 eV ($E_{loss}$) [60] than that of the **PTBTHD-IDEH** device (1.0 eV). However, the **PTBTEH-IDHD** device shows the smallest $V_{oc}$ value (0.71 V) though its HOMO energy level is equal to −5.47 eV, and its $E_{loss}$ (1.28 eV) is larger than the others. It could be attributed to the serious phase separation morphology of the **PTBTEH-IDHD** blend film which leads to increased interface trap states and charge carrier recombination derived from a low effective interfacial area [61].

As mentioned before, the **PTBTEH-IDHD** blend film possesses the most serious phase separation, the largest domain size and the lowest mobility of $4.2 \times 10^{-7}$ $cm^2$ $V^{-1}$ $s^{-1}$, which would certainly result in the most serious charge recombination and imbalance between hole mobility and electron mobility in the blend film. Therefore, the **PTBTEH-IDHD** device only exhibits the lowest FF value of 0.35. On the contrary, the **PTBTOD-IDB** blend film

**Table 3**
Photovoltaic properties of the PSC devices and hole mobility of the blend film (polymers: $PC_{71}BM$ = 1: 1.5, w/w; 97.6% *o*-DCB +2.4%DIO).

| Polymer | $J_{sc}$ (mA $cm^{-2}$) | $V_{oc}$ (V) | FF | $PCE_{max}$ ($PCE_{ave}$) (%) | $\mu_{h,\ ave}$ ($cm^2$ $V^{-1}$ $s^{-1}$) |
|---|---|---|---|---|---|
| **PTBTEH-IDHD** | 2.68 | 0.71 | 0.35 | 0.67(0.44) | $4.2 \times 10^{-7}$ |
| **PTBTHD-IDEH** | 10.11 | 0.87 | 0.43 | 3.79(3.50) | $3.4 \times 10^{-5}$ |
| **PTBTOD-IDB** | 11.66 | 0.81 | 0.56 | 5.29(5.09) | $2.5 \times 10^{-4}$ |

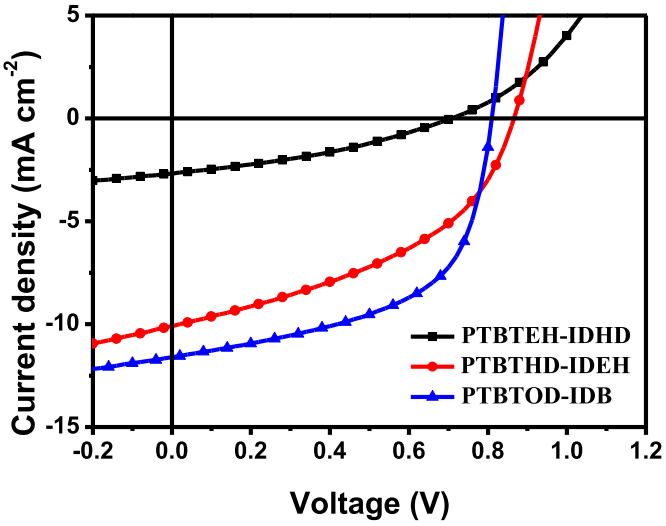


**Fig. 7.** *J-V* curves of the PSCs based on the polymers under the illumination of AM 1.5G, 100 mW $cm^{-2}$.

possesses the most appropriate microphase separation, the smallest domain size, and the highest hole mobility ($2.5 \times 10^{-4}$ $cm^2$ $V^{-1}$ $s^{-1}$), which result in less charge recombination and a relatively balanced hole mobility and electron mobility in the film than the others. Consequently, the **PTBTOD-IDB** device achieves the highest FF values of 0.56.

As discussed before, **PTBTEH-IDHD** possesses the lowest absorbance in the film, the weakest π−π stacking interaction and crystallization ability, the most inferior electron transport ability to $PC_{71}BM$, the largest microphase separation with $PC_{71}BM$ and the lowest hole mobility, so the **PTBTEH-IDHD**-based PSC device only shows the lowest $J_{sc}$ of 2.68 mA $cm^{-2}$. However, **PTBTOD-IDB** shows the largest light harvesting capacity, the strongest π−π stacking interaction and crystallization ability, the most effective electron transport ability to $PC_{71}BM$, the most appropriate microphase separation with $PC_{71}BM$ and the highest hole mobility, so the **PTBTOD-IDB**-based PSC device shows the highest $J_{sc}$ value of 11.66 mA $cm^{-2}$. Obviously, the $J_{sc}$ value increases with the prolongation of the side chain on the TBT unit and shrinkage of the side chain on isoindigo unit. The incident photon-to-current conversion efficiencies (IPCE) curves give the similar results (Fig. 8). The PSC devices based on these polymers show an IPCE response between 300 and 800 nm, and the devices show the maximum IPCE value 14.8% at 345 nm for **PTBTEH-IDHD**, 44.7% at 625 nm for **PTBTHD-IDEH**, 57.2% at 466 nm for **PTBTOD-IDB**. The $J_{sc}$ values, calculated from the IPCE results, are 2.29 mA $cm^{-2}$ for **PTBTEH-IDHD**, 9.68 mA $cm^{-2}$ for **PTBTHD-IDEH**, and 10.89 mA $cm^{-2}$ for **PTBTOD-IDB**, which are nearly in accord with the measured $J_{sc}$ values within experimental error. As a result, the PSC devices exhibit the PCE values of 0.67% for **PTBTEH-IDHD**, 3.79% for **PTBTHD-IDEH**, and 5.29% for **PTBTOD-IDB**.

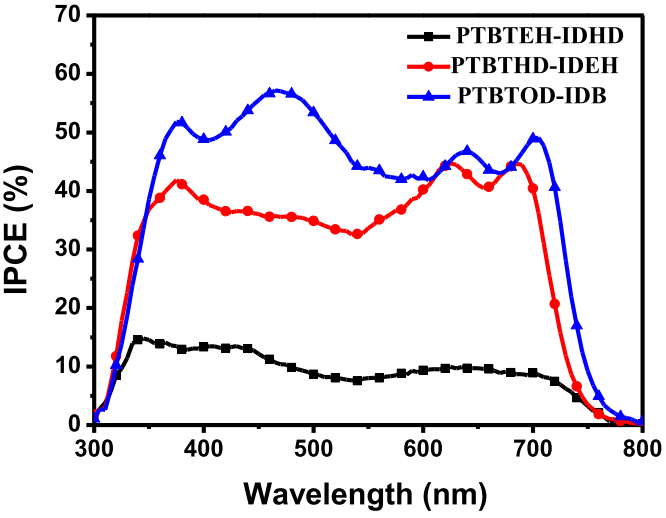


**Fig. 8.** IPCE curves of the PSCs based on the polymers.

## 4. Conclusions

In summary, three conjugated polymers with a different alkyl chain length on the TBT moieties and isoindigo moieties have been designed and synthesized, in which the side chain in a constitutional repeating unit is fixed as $C_{48}H_{100}$. The results indicate that the polymer **PTBTOD-IDB**, with the longest side chain (2-octyldodecyl) on TBT and the shortest side chain (*n*-butyl) on ID, shows stronger interchain interaction and light-harvesting capacity in *o*-DCB solution and thin film, lower band gap, stronger π−π stacking interaction, more appropriate microphase separation with $PC_{71}BM$, higher hole mobility and better photovoltaic performance than the other polymers. This study not only fully investigates the length effect of the alkyl side chains on the photovoltaic performance, but also thoroughly avoids the negative deviation that the different carbon atom number of the side chain in a constitutional repeating unit leads to solubility and morphology variance. Therefore, it affords a favorable evidence that the polymer with long branched side chain on D moieties and short linear side chain on A moieties possesses stronger molecular aggregation, better morphology, and higher photovoltaic performance.

## Acknowledgements

This work was supported by the National Natural Science Foundation of China (51573153), the Natural Science Foundation of Hunan Province of China (2015JJ2141) and the Scientific Research Fund of Hunan Provincial Education Department (15A180).

## Appendix A. Supplementary data

Supplementary data related to this article can be found at http://dx.doi.org/10.1016/j.dyepig.2016.12.036.

## References

[1] Zhong C, Bartelt JA, McGehee MD, Cao D, Huang F, Cao Y, et al. Influence of intermixed donor and acceptor domains on the ultrafast charge generation in bulk heterojunction materials. J Phys Chem C 2015;119(48):26889–94.
[2] Wang K, Guo B, Xu Z, Guo X, Zhang MJ, Li YF. Solution-processable organic molecule for high-performance organic solar cells with low acceptor content. ACS Appl Mater Interfaces 2015;7(44):24686–93.
[3] Dou LT, Gao J, Richard E, You JB, Chen CC, Cha KC, et al. Systematic investigation of benzodithiophene- and diketopyrrolopyrrole-based low-bandgap polymers designed for single junction and tandem polymer solar cells. J Am Chem Soc 2012;134(24):10071–9.
[4] Guo H, Shen TP, Wu F, Wang G, Ye LL, Liu ZX, et al. Controlling the morphology and hole mobility of terpolymers for polymer solar cells. RSC Adv 2016;6(16):13177–84.
[5] Lin YZ, Zhao FW, He Q, Huo LJ, Wu Y, Parker TC, et al. High-performance electron acceptor with thienyl side chains for organic photovoltaics. J Am Chem Soc 2016;138(14):4955–61.
[6] Bin HJ, Zhang ZG, Gao L, Chen SS, Zhong L, Xue LW, et al. Non-fullerene polymer solar cells based on alkylthio and fluorine substituted 2D-conjugated polymers reach 9.5% efficiency. J Am Chem Soc 2016;138(13):4657–64.
[7] Zhao WC, Qian DP, Zhang SQ, Li SS, Inganas O, Gao F, et al. Fullerene-free polymer solar cells with over 11% efficiency and excellent thermal stability. Adv Mater 2016;28(23):4734–9.

[8] Nguyen TL, Choi H, Ko SJ, Uddin MA, Walker B, Yum S, et al. Semi-crystalline photovoltaic polymers with efficiency exceeding 9% in a ~300 nm thick conventional single-cell device. Energy Environ Sci 2014;7(9):3040–51.
[9] Yang YK, Zhang ZG, Bin HJ, Chen SS, Gao L, Xue LW, et al. Side-chain isomerization on n-type organic semiconductor ITIC acceptor make 11.77% high efficiency polymer Solar Cells. J Am Chem Soc 2016;138(45):15011–8.
[10] Bin HJ, Gao L, Zhang ZG, Yang YK, Zhang YD, Zhang CF, et al. 11.4% Efficiency non-fullerene polymer solar cells with trialkylsilyl substituted 2D-conjugated polymer as donor. Nat Commun 2016;7:13651.
[11] Xu YX, Chueh CC, Yip HL, Ding FZ, Li YX, Li CZ, et al. Improved charge transport and absorption coefficient in indacenodithieno 3,2-b thiophene-based ladder-type polymer leading to highly efficient polymer solar cells. Adv Mater 2012;24(47):6356–61.
[12] Li YX, Yao K, Yip HL, Ding FZ, Xu YX, Li XS, et al. Eleven-membered fused-ring low band-gap polymer with enhanced charge carrier mobility and photovoltaic performance. Adv Funct Mater 2014;24(23):3631–8.
[13] Zhang MJ, Guo X, Li YF. Photovoltaic performance improvement of D–A copolymers containing bithiazole acceptor unit by using bithiophene bridges. Macromolecules 2011;44(22):8798–804.
[14] Li YF. Molecular design of photovoltaic materials for polymer solar cells: toward suitable electronic energy levels and broad absorption. Acc Chem Res 2012;45(5):723–33.
[15] Li CZ, Chueh CC, Ding FZ, Yip HL, Liang PW, Li XS, et al. Doping of fullerenes via anion-induced electron transfer and its implication for surfactant facilitated high performance polymer solar cells. Adv Mater 2013;25(32):4425–30.
[16] Tan ZA, Li LJ, Wang FZ, Xu Q, Li SS, Sun G, et al. Solution-processed rhenium oxide: a versatile anode buffer layer for high performance polymer solar cells with enhanced light harvest. Adv Energy Mater 2014;4(1):1300884.
[17] Guo X, Zhang MJ, Ma W, Ye L, Zhang SQ, Liu SJ, et al. Enhanced photovoltaic performance by modulating surface composition in bulk heterojunction polymer solar cells based on PBDTTT-C-T/PC71BM. Adv Mater 2014;26(24):4043–9.
[18] Yang D, Zhou LY, Yu W, Zhang J, Li C. Work-function-tunable chlorinated graphene oxide as an anode interface layer in high-efficiency polymer solar cells. Adv Energy Mater 2014;4(15):1400591.
[19] Wang EG, Mammo W, Andersson MR. 25th Anniversary article: isoindigo-based polymers and small molecules for bulk heterojunction solar cells and field effect transistors. Adv Mater 2014;26(12):1801–26.
[20] Wang CW, Zhao B, Cao ZC, Shen P, Tan Z, Li XL, et al. Enhanced power conversion efficiencies in bulk heterojunction solar cells based on conjugated polymer with isoindigo side chain. Chem Commun 2013;49(37):3857–9.
[21] Fang L, Zhou Y, Yao YX, Diao Y, Lee WY, Appleton AL, et al. Side-chain engineering of isoindigo-containing conjugated polymers using polystyrene for high-performance bulk heterojunction solar cells. Chem Mater 2013;25(24):4874–80.
[22] Wang EG, Ma ZF, Zhang Z, Vandewal K, Henriksson P, Inganas O, et al. An easily accessible isoindigo-based polymer for high-performance polymer solar cells. J Am Chem Soc 2011;133(36):14244–7.
[23] Mahmood K, Liu ZP, Li CH, Lu Z, Fang T, Liu X, et al. Novel isoindigo-based conjugated polymers for solar cells and field effect transistors. Polym Chem 2013;4(12):3563–74.
[24] Ma ZF, Dang DF, Tang Z, Gedefaw D, Bergqvist J, Zhu WG, et al. A facile method to enhance photovoltaic performance of benzodithiophene-isoindigo polymers by inserting bithiophene spacer. Adv Energy Mater 2014;4(6):1301455.
[25] Deng YF, Liu J, Wang JT, Liu LH, Li WL, Tian HK, et al. Dithienocarbazole and isoindigo based amorphous low bandgap conjugated polymers for efficient polymer solar cells. Adv Mater 2013;26(3):471–6.
[26] Yang LQ, Zhou HX, You W. Quantitatively analyzing the influence of side chains on photovoltaic properties of polymer-fullerene solar cells. J Phys Chem C 2010;114(39):16793–800.
[27] Zhang ZG, Li YF. Side-chain engineering of high-efficiency conjugated polymer photovoltaic materials. Sci China Chem 2015;58(2):192–209.
[28] Nishinaga S, Mori H, Nishihara Y. Impact of alkyl side chains on thin-film transistor performances in phenanthrodithiophene–isoindigo copolymers. Chem Lett 2015;44(7):998–1000.
[29] Ma ZY, Geng H, Wang D, Shuai ZG. Influence of alkyl side-chain length on the carrier mobility in organic semiconductors: herringbone vs. π-π stacking. J Mater Chem C 2016;4(20):4546–55.
[30] Dang DF, Chen WC, Himmelberger S, Tao Q, Lundin A, Yang RQ, et al. Enhanced photovoltaic performance of indacenodithiophene-quinoxaline copolymers by side-chain modulation. Adv Energy Mater 2014;4(15):1400680.
[31] Meager I, Ashraf RS, Mollinger S, Schroeder BC, Bronstein H, Beatrup D, et al. Photocurrent enhancement from diketopyrrolopyrrole polymer solar cells through alkyl-chain branching point manipulation. J Am Chem Soc 2013;135(31):11537–40.
[32] Lu LY, Zheng TX, Wu Q, Schneider AM, Zhao DL, Yu LP. Recent advances in bulk heterojunction polymer solar cells. Chem Rev 2015;115(23):12666–731.
[33] Liu Y, Zhao J, Li Z, Mu C, Ma W, Hu H, et al. Aggregation and morphology control enables multiple cases of high-efficiency polymer solar cells. Nat Commun 2014;5:5293–300.
[34] Bronstein H, Leem DS, Hamilton R, Woebkenberg P, King S, Zhang WM, et al. Indacenodithiophene-co-benzothiadiazole copolymers for high performance solar cells or transistors via alkyl chain optimization. Macromolecules 2011;44(17):6649–52.
[35] Shin J, Park GE, Lee DH, Um HA, Lee TW, Cho MJ, et al. Bis(thienothiophenyl) diketopyrrolopyrrole-based conjugated polymers with various branched alkyl side chains and their applications in thin-film transistors and polymer solar cells. ACS Appl Mater Interfaces 2015;7(5):3280–8.
[36] Constantinou I, Lai TH, Klump ED, Goswami S, Schanze KS, So F. Effect of polymer side chains on charge generation and disorder in PBDTTPD solar cells. ACS Appl Mater Interfaces 2015;7(48):26999–7005.
[37] Han AR, Lee J, Lee HR, Lee J, Kang S-H, Ahn H, et al. Siloxane side chains: a universal tool for practical applications of organic field-effect transistors. Macromolecules 2016;49(10):3739–48.
[38] Xu ZS, Luo GP, Yu JS, Yin XX, Zhu EW, Zhang FJ, et al. Side-chain manipulation on accepting units of two-dimensional benzo [1,2-b:4,5-b′] dithiophene polymers for organic photovoltaics. Polym Chem 2016;7(7):1486–93.
[39] Yuan JY, Dong HL, Li M, Huang XD, Zhong J, Li YY, et al. High polymer/fullerene ratio realized in efficient polymer solar cells by tailoring of the polymer side-chains. Adv Mater 2014;26(22):3624–30.
[40] Nishinaga S, Mori H, Nishihara Y. Phenanthrodithiophene–isoindigo copolymers: effect of side chains on their molecular order and solar cell performance. Macromolecules 2015;48(9):2875–85.
[41] Graham KR, Cabanetos C, Jahnke JP, Idso MN, El Labban A, Ngongang Ndjawa GO, et al. Importance of the donor:fullerene intermolecular arrangement for high-efficiency organic photovoltaics. J Am Chem Soc 2014;136(27):9608–18.
[42] Zhou HX, Yang LQ, Stuart AC, Price SC, Liu SB, You W. Development of fluorinated benzothiadiazole as a structural unit for a polymer solar cell of 7% efficiency. Angew Chem Int Ed. 2011;123(13):3051–4.
[43] Lee D, Hubijar E, Kalaw GJD, Ferraris JP. Enhanced and tunable open-circuit voltage using dialkylthio benzo[1,2-b:4,5-b′]dithiophene in polymer solar cells. Chem Mater 2012;24(13):2534–40.
[44] Cui CH, Wong WY, Li YF. Improvement of open-circuit voltage and photovoltaic properties of 2D-conjugated polymers by alkylthio substitution. Energy Environ Sci 2014;7(7):2276–84.
[45] Ye L, Zhang SQ, Zhao WC, Yao HF, Hou JH. Highly efficient 2D-conjugated benzodithiophene-based photovoltaic polymer with linear alkylthio side chain. Chem Mater 2014;26(12):3603–5.
[46] Zhang ZG, Min J, Zhang SY, Zhang J, Zhang MJ, Li YF. Alkyl chain engineering on a dithieno[3,2-b:2′,3′-d]silole-alt-dithienylthiazolo[5,4-d]thiazole copolymer toward high performance bulk heterojunction solar cells. Chem Commun 2011;47(33):9474–6.
[47] Zhang MJ, Guo X, Li YF. Synthesis and characterization of a copolymer based on thiazolothiazole and dithienosilole for polymer solar cells. Adv Energy Mater 2011;1(4):557–60.
[48] Hou RY, Zhao B, Wu F, Wang G, Shen TP, Guo H, et al. Synthesis, characterization, and photovoltaic performance of the polymers based on thiophene-2,5-bis((2-ethylhexyl)oxy) benzene-thiophene. Org Electron 2015;20:142–9.
[49] Zhang GB, Fu YY, Xie ZY, Zhang Q. Synthesis and photovoltaic properties of new low bandgap isoindigo-based conjugated polymers. Macromolecules 2011;44(6):1414–20.
[50] Hermet P, Lois-Sierra S, Bantignies J-L, Rols S, Sauvajol J-L, Serein-Spirau F, et al. Lattice dynamics of oligo(phenylenethienylene)s: a far-infrared and inelastic neutron scattering study. J Phys Chem B 2009;113(13):4197–202.
[51] Stalder R, Mei JG, Graham KR, Estrada LA, Reynolds JR. Isoindigo, a versatile electron-deficient unit for high-performance organic electronics. Chem Mater 2014;26(1):664–78.
[52] Huang YS, Zhang M, Chen HJ, Wu F, Cao ZC, Zhang LJ, et al. Efficient polymer solar cells based on terpolymers with a broad absorption range of 300–900 nm. J Mater Chem A 2014;2(15):5218–23.
[53] Gu ZJ, Tang P, Zhao B, Luo H, Guo X, Chen HJ, et al. Synthesis and photovoltaic properties of copolymers based on benzo[1,2-b:4,5-b′]dithiophene and thiophene with different conjugated side groups. Macromolecules 2012;45(5):2359–66.
[54] Liu YH, Zhao JB, Li ZK, Mu C, Ma W, Hu HW, et al. Aggregation and morphology control enables multiple cases of high-efficiency polymer solar cells. Nat Commun 2014;5:5293–300.
[55] Fan QP, Liu Y, Mj Xiao, Tan H, Wang YF, Su WY, et al. Donor–acceptor copolymers based on benzo[1,2-b:4,5-b′]dithiophene and pyrene-fused phenazine for high-performance polymer solar cells. Org Electron 2014;15(11):3375–83.
[56] Cheng Y-J, Yang S-H, Hsu C-S. Synthesis of conjugated polymers for organic solar cell applications. Chem Rev 2009;109(11):5868–923.
[57] Wang Y, Yang F, Liu Y, Peng RX, Chen SJ, Ge ZY. New alkylfuranyl-substituted benzo[1,2-b:4,5-b′]dithiophene-based donor–acceptor polymers for highly efficient solar cells. Macromolecules 2013;46(4):1368–75.
[58] Zhao B, Li CZ, Liu SQ, Richards JJ, Chueh CC, Ding FZ, et al. A conductive liquid crystal via facile doping of an n-type benzodifurandione derivative. J Mater Chem A 2015;3(13):6929–34.
[59] Guo X, Cui CH, Zhang MJ, Huo LJ, Huang Y, Hou JH, et al. High efficiency polymer solar cells based on poly(3-hexylthiophene)/indene-C70 bisadduct with solvent additive. Energy Environ Sci 2012;5(7):7943–9.
[60] Gao K, Li L, Lai T, Xiao L, Huang Y, Huang F, et al. Deep absorbing porphyrin small molecule for high-performance organic solar cells with very low energy losses. J Am Chem Soc 2015;137(23):7282–5.
[61] Elumalai NK, Uddin A. Open circuit voltage of organic solar cells: an in-depth review. Energy Environ Sci 2016;9(2):391–410.